NAG-3-546

Mechanical Engineering Department
University of Wisconsin--Milwaukee
Milwaukee, Wisconsin 53201

A STUDY OF REYNOLDS-STRESS CLOSURE MODEL

Semi-Annual Progress Report

January 1985

by

R. S. Amano
Principal Investigator

and

P. Goel
Research Assistant

The report documents research completed during the period of June 1, 1984 thru January 15, 1985 under NASA-Lewis Research Grant NO. NAG 3-546.

TF/85/1

ABSTRACT

The report outlines progress of the research conducted during the period of June 1984-January 1985. During this period items 2.1, 2.2 and 2.5 in the project proposal have been mostly accomplished. Moreover, a closure of third-order was pursued to improve the diffusion rate of the Reynolds-stress transport equations for the prediction of recirculating and reattaching flows.

TABLE OF CONTENTS

NOMENCLATURE

B_1, B_2, B_3	constants used in turbulence model
C_1, C_2, C_3, C_D, C_s, $C_{\varepsilon 1}$, $C_{\varepsilon 2}$, C_μ	coefficients used in turbulence model
D_{ij}	diffusion of $\overline{u_i u_j}$
G	generation rate of turbulence kinetic energy, k
H	step height
k	turbulence kinetic energy
p	pressure fluctuation
P	mean pressure
P_{ij}	generation rate of Reynolds stresses
Q_{ij}	generation rate used in pressure-strain correlation
Re_θ	Reynolds number based on momentum thickness, θ
u	fluctuating velocity
U	mean velocity
U_{IN}	mean velocity at the inlet
U_τ	friction velocity ($=\sqrt{\tau_w/\rho}$)
v	fluctuating velocity in y-direction
V	mean velocity in y-direction
x	Cartesian coordinate
x_r	length of reattachment
y	Cartesian coordinate
Y_o	height of inlet flow section
z	coordinate normal to the wall
δ_{ij}	Kronecker delta
δA	area of numerical cell
ε	energy dissipation rate

c_x	grid expansion factor in x-direction
μ	dynamic molecular viscosity
ρ	density
σ_k, σ_ε	Prandtl numbers for k and ε
τ_w	wall shear stress
Φ_{ij}	pressure-strain correlation

Subscripts

i, j, k, ℓ, m	tensor notations
w	wall values

1. INTRODUCTION

Flow in a channel which has steps or sharp bends occurs in many engineering applications, such as airfoils with separation bubbles, combustors, heat exchangers, etc. While there have been significant contributions in this field, current understanding of the process is still relatively poor, partly because the flow in these geometries is complex, and partly because theoretical models developed to date are limited in predicting a wide range of parameters in separating, reattaching, and recirculating flows.

Bradshaw and Wong[1] and Smyth[2] measured turbulence quantities in the reattaching and redeveloping regions and reported that the center part of the reattaching shear-layer still has most of the characteristics of a free shear layer as many as 50 step heights downstream of the reattachment point. This suggests that the large-scale eddies that develop in the separated free shear layer persist in the reattaching and redeveloping regions. However, the turbulent shear stress in the reattaching layer is much larger than the shear stress in an ordinary plane-mixing layer and it decreases rapidly near the reattachment point.

Eaton and Johnston[3] focused measurement on the separated flow over the backward-facing step. A comparison with a plane-mixing layer showed that the normal components of Reynolds stresses in the shear layer near the reattachment point were 10-20% higher than typical values measured in plane-mixing layers. However, the values of shear stress were of about the same order as those of plane-mixing layers in most of the region upstream of the reattachment. It was also shown that the reattaching layer was similar to a plane mixing layer downstream of the reattachment region. These observations indicate that many parameters could be predicted in the reattaching shear layer by

using simple mixing-layer data; and, consequently, the turbulence models used in a mixing-layer flow would still be adequate for the reattaching shear layer.

Theoretical studies for turbulence modeling for a wide range of flow patterns are available. Among the existing models, the so-called Reynolds-stress model of turbulence, which consists of transport equations for all the Reynolds stresses, provides individual stress behaviors, while the viscosity based-models like the $k \sim \varepsilon$ model cannot account for such behaviors because an isotropic assumption is used. A model of the Reynolds stresses was first proposed by Rotta[4], and has been developed and improved by a number of researchers.[5-8] The correlation of pressure-strain was proposed by Naot et al.[6] and Launder et al.[8] Naot et al. evaluated the pressure-strain correlation term by integrating over space after inserting a conjectured form for the two-point correlation functions, whereas Launder et al. obtained the results by assuming a fourth-order tensor consisting of linear Reynolds-stress elements. As a simplified model of the Reynolds-stress closure model, an algebraic stress model which does not possess both convection and diffusion terms was developed in a similar manner by Rodi.[9]

In the authors' previous paper[10] several proposed closures for the Reynolds-stress model were tested for heat transfer characteristics along walls of axisymmetric sudden expansion pipes. After computation using several different models, it was found that the pressure-strain correlation proposed by Launder et al.[8] showed slightly better agreement with experimental data for Nusselt number distributions along the pipe walls. Moreover, an incorporation of the wall correction terms in the pressure-strain also improved predictions by about 5 to 10 percent.

Although the Reynolds-stress closure model (RSM)* was formulated in the previous work[10], the behavior of the stress components was not examined due to a lack of suitable experimental data on the Reynolds stresses. In this study the previous model was reviewed again, and Reynolds-stress levels computed by the model presently developed were compared with experimental data available in the literature. The results of the Reynolds-stress levels were also compared with the computations obtained by using the standard $k \sim \varepsilon$ model and the algebraic stress model.

Meanwhile, the authors also noticed the fact that the triple velocity products in the separated shear layer begin to show a marked drop in the near-reattachment region due to a suppression of the large-scale eddies as the flow approaches a solid wall. This indicates that the third-order tensor quantities, which have direct influence on the diffusive action of the Reynolds stresses, must be evaluated carefully for a reattaching shear layer. This study was added to the proposed research before the Reynolds stress model is extended further for heat transfer problems. In this way the diffusion rate of the second-order closure model of the Reynolds stresses will eventually be treated by the third-order closure model. The mathematical formulation of all the models is described in the following section.

2. MATHEMATICAL FORMULATION

The steady, two-dimensional form of continuity and momentum equations describing the flow field are used in this study. These are given as:

---

*This is not the complete Reynolds-stress model because the stresses in the momentum equations were evaluated by using the Boussinesq viscosity model.

Continuity Equation:

$$\frac{\partial}{\partial x_j}(\rho U_j) = 0 \tag{1}$$

Momentum Equation:

$$\frac{\partial}{\partial x_j}(\rho U_i U_j) = -\frac{\partial P}{\partial x_i} + \frac{\partial}{\partial x_j}[\mu(\frac{\partial U_i}{\partial x_j} + \frac{\partial U_j}{\partial x_i}) - \rho\overline{u_i u_j}] \tag{2}$$

2.1 Reynolds-Stress Equations

If the Reynolds stresses, $\overline{u_i u_j}$, were computed through the solution of the Reynolds stress transport equations, these values could be simply inserted into Eq. (2); and the final flow field could be obtained by solving Eqs. (1) and (2) and the Reynolds-stress equations iteratively. However, considerable difficulty was encountered in solving the momentum equations due to the numerically unstable nature of these equations. Since the Reynolds stresses, $\rho\overline{u_i u_j}$, in Eq. (2) are evaluated through the source terms of the discretization equations, the diffusion term of the momentum equations contains only molecular diffusion rates. Consequently the convection rate of the momentum predominates over the diffusion rate, causing inherent instability in the solution. This problem is overcome by bringing the Reynolds stresses into the diffusion term with a suitable modification. However, since this modification has been successfully carried out just recently and is still in the testing process for universal usage, the conventional Boussinesq effective viscosity was tentatively adopted to demonstrate the models developed so far. The description of the new diffusion part is given in the "WORK IN PROGRESS" section at the end of this report (Sec. 6.2).

The closure of the Reynolds stresses in Eq. (2) was achieved as follows:

$$-\rho\overline{u_i u_j} = C_\mu \frac{\rho k^2}{\varepsilon}\left(\frac{\partial U_i}{\partial x_j} + \frac{\partial U_j}{\partial x_i}\right) - \frac{2}{3}\delta_{ij}\rho k \tag{3}$$

where k and ε are obtained by solving the standard k ~ ε model as shown below.

$$\frac{\partial}{\partial x_j}(\rho U_j k) = \rho(G - \varepsilon) + \frac{\partial}{\partial x_j}\left[\left(\mu + \frac{C_\mu \rho k^2}{\sigma_k \varepsilon}\right)\frac{\partial k}{\partial x_j}\right] \tag{4}$$

$$\frac{\partial}{\partial x_j}(\rho U_j \varepsilon) = \frac{\rho\varepsilon}{k}\left(C_{\varepsilon_1} G - C_{\varepsilon_2}\varepsilon\right) + \frac{\partial}{\partial x_j}\left[\left(\mu + \frac{C_\mu \rho k^2}{\sigma_\varepsilon \varepsilon}\right)\frac{\partial \varepsilon}{\partial x_j}\right] \tag{5}$$

Here the generation rate of the turbulence kinetic energy can be expressed as

$$G = -\overline{u_i u_j}\frac{\partial U_i}{\partial x_j} \tag{6}$$

The values for the constants used above are given as

C_μ	$C_{\varepsilon 1}$	$C_{\varepsilon 2}$	σ_k	σ_ε
0.09	1.44	1.92	1.00	1.30

The transport equations for the Reynolds stresses are given as

$$\frac{\partial}{\partial x_k}\left(U_k \overline{u_i u_j}\right) = P_{ij} - \varepsilon_{ij} + \Phi_{ij} + \Phi_{ij,w} + D_{ij} \tag{7}$$

where

$$P_{ij} = -\left(\overline{u_j u_k}\frac{\partial U_i}{\partial x_k} + \overline{u_i u_k}\frac{\partial U_j}{\partial x_k}\right) \quad : \text{ generation} \tag{8}$$

$$\varepsilon_{ij} = 2\nu \overline{\frac{\partial u_i}{\partial x_k} \frac{\partial u_j}{\partial x_k}} \quad : \text{ dissipation} \tag{9}$$

$$\Phi_{ij} = \overline{\frac{p}{\rho} \left(\frac{\partial u_i}{\partial x_j} + \frac{\partial u_j}{\partial x_i}\right)} \quad : \text{ pressure-strain correlation} \tag{10}$$

and

$$D_{ij} = -\frac{\partial}{\partial x_k} \left(\overline{u_i u_j u_k}\right) \quad : \text{ diffusion} \tag{11}$$

Equation (9) was approximated by the form given by Rotta[4] as:

$$\varepsilon_{ij} = \frac{2}{3} \delta_{ij} \varepsilon \tag{12}$$

The pressure strain term (10) was determined combining Rotta's[4] linear return-to-isotropy hypothesis and the linear approximation of Launder et al.[8] The results are given as:

$$\begin{aligned} \Phi_{ij} = &-C_1 \varepsilon \left(\frac{\overline{u_i u_j}}{k} - \frac{2}{3} \delta_{ij}\right) - B_1 \left(P_{ij} - \frac{2}{3} \delta_{ij} G\right) \\ &-B_2 k \left(\frac{\partial U_i}{\partial x_j} + \frac{\partial U_j}{\partial x_i}\right) - B_3 \left(Q_{ij} - \frac{2}{3} \delta_{ij} G\right) \end{aligned} \tag{13}$$

where

$$\begin{aligned} &B_1 = (C_2 + 8)/11, \; B_2 = (30C_2 - 2)/55, \; B_3 = (8C_2 - 2)/11 \\ &C_1 = 1.5, \; C_2 = 0.4 \end{aligned} \tag{14}$$

and

$$Q_{ij} = -(\overline{u_i u_k}\,\frac{\partial U_k}{\partial x_j} + \overline{u_j u_k}\,\frac{\partial U_k}{\partial x_i}) \tag{15}$$

The pressure-strain correlation with a near-wall correction* is given as

$$\phi_{ij,w} = [0.125\,\frac{\varepsilon}{k}(\overline{u_i u_j} - \frac{2}{3}\,k\delta_{ij}) + 0.015(P_{ij} - Q_{ij})]\,\frac{k^{\frac{3}{2}}}{\varepsilon z} \tag{16}$$

where z is a coordinate taken normal to the wall. Thus, if the point of interest is close to two plates (say z_1 to one plate and z_2 to the other), then z is chosen to be

$$z = 1/(1/z_1 + 1/z_2) \tag{17}$$

The diffusion rate (11) is evaluated as:

$$D_{ij} = C_D\,\frac{\partial}{\partial x_k}(\,\frac{k}{\varepsilon}\,\overline{u_k u_m}\,\frac{\partial \overline{u_i u_j}}{\partial x_m}\,) \tag{18}$$

where C_D is a constant with a value of 0.25 which was determined by computer optimization.

It should be noted that both convection and diffusion rates of the Reynolds stresses are neglected in the so-called algebraic stress model (ASM) whereas they are kept in the present RSM.

---

*Although this correlation was used for the computation of the Reynolds stresses, the contribution of this term was relatively minor. That is why this term was dropped when the triple velocity products were computed.

2.2 Third-Order Closure Model

In view of the discussion given in the last part of the introduction section, the triple velocity fluctuation products, $\overline{u_i u_j u_k}$, should be evaluated appropriately in a separating and reattaching flow region. This may be attained by formulating transport equations that solve for $\overline{u^3}$, $\overline{u^2 v}$, $\overline{uv^2}$ and $\overline{v^3}$. The brief procedure of formulation and its closure model is given as follows.

The general transport equation can be derived by suitable multiplication of the transport equation for a single fluctuating velocity u by unaveraged Reynolds stresses. Then, after time averaging of the resultant equation, the following is obtained.

$$\overline{u_j u_k \frac{Du_i}{Dt}} + \overline{u_k u_i \frac{Du_j}{Dt}} + \overline{u_i u_j \frac{Du_k}{Dt}} = \frac{D\overline{u_i u_j u_k}}{Dt} \tag{19}$$

This will lead us to the transport equation of $\overline{u_i u_j u_k}$ as

$$\begin{aligned}
\frac{D\overline{u_i u_j u_k}}{Dt} = & - [\overline{u_i u_j u_\ell} \frac{\partial U_k}{\partial x_\ell} + \overline{u_j u_k u_\ell} \frac{\partial U_i}{\partial x_\ell} + \overline{u_k u_i u_\ell} \frac{\partial U_j}{\partial x_\ell}] \\
& \qquad \text{(I)} \\
& + [\overline{u_i u_j} \frac{\overline{\partial u_k u_\ell}}{\partial x_\ell} + \overline{u_j u_k} \frac{\overline{\partial u_i u_\ell}}{\partial x_\ell} + \overline{u_k u_i} \frac{\overline{\partial u_j u_\ell}}{\partial x_\ell}] \\
& \qquad \text{(II)} \\
& - \frac{\partial}{\partial x_\ell} [\overline{u_i u_j u_k u_\ell}] \\
& \qquad \text{(III)} \\
& - \frac{1}{\rho} [\overline{u_i u_j \frac{\partial p}{\partial x_k}} + \overline{u_j u_k \frac{\partial p}{\partial x_i}} + \overline{u_k u_i \frac{\partial p}{\partial x_j}}] \\
& \qquad \text{(IV)}
\end{aligned} \tag{20}$$

In closing Eq. (20), we need to make some assumptions. Because the first and second terms (I and II) on the RHS consist of mean strains, stresses, and triple products, they can be evaluated directly without making any correlation. The third term contains quadruple velocity fluctuation products, and these must be correlated in terms of known quantities such as the Reynolds stresses or mean strain rates. Millionshtchikov[11] assumed that the quadruple velocity correlations are Gaussian and thus approximated them by using the product of the second-order correlations obtained by the formulae which are strictly fulfilled for the normal law. Then the quadruple velocity product can be decoupled as

$$\overline{u_i u_j u_k u_\ell} = \overline{u_i u_j} \cdot \overline{u_k u_\ell} + \overline{u_i u_k} \cdot \overline{u_j u_\ell} + \overline{u_i u_\ell} \cdot \overline{u_k u_j} \tag{21}$$

and, hence, the sum of terms II and III is finally rearranged as

$$II + III = - \left[\overline{u_i u_\ell} \frac{\partial \overline{u_j u_k}}{\partial x_\ell} + \overline{u_j u_\ell} \frac{\partial \overline{u_k u_i}}{\partial x_\ell} + \overline{u_k u_\ell} \frac{\partial \overline{u_i u_j}}{\partial x_\ell}\right] \tag{22}$$

The last term (IV) can be correlated with the triple correlation as

$$IV = -C_s \frac{\varepsilon}{k} \overline{u_i u_j u_k} \tag{23}$$

where the coefficient C_s needs to be determined by a computer optimization technique. Through our preliminary examination, it is found that the computations with C_s values of between 1.0 and 10.0 result in acceptable levels of $\overline{u_i u_j u_k}$.

With the approximation mentioned above, Eq. (20) is finally written as

$$\frac{D\overline{u_i u_j u_k}}{Dt} = -\left[\overline{u_i u_j u_k}\frac{\partial U_k}{\partial x_\ell} + \overline{u_j u_k u_\ell}\frac{\partial U_i}{\partial x_\ell} + \overline{u_k u_i u_\ell}\frac{\partial U_j}{\partial x_\ell}\right]$$

$$-\left[\overline{u_i u_\ell}\frac{\partial \overline{u_j u_k}}{\partial x_\ell} + \overline{u_j u_\ell}\frac{\partial \overline{u_k u_i}}{\partial x_\ell} + \overline{u_k u_\ell}\frac{\partial \overline{u_i u_j}}{\partial x_\ell}\right] \qquad (24)$$

$$-C_s\frac{\varepsilon}{k}\overline{u_i u_j u_k}$$

2.3 Other Models of Third-Order Closure

The transport model of the third-order velocity products described in the preceding section was developed along with other existing models for the flow field of reattaching shear layer. In this section these other models are discussed.

Daly and Harlow[5] obtained an algebraic expression with a simplification of such a transport equation of $\overline{u_i u_j u_k}$ as follows

$$\overline{u_i u_j u_k} = -2.0\, C_3 \frac{k}{\varepsilon}\overline{u_k u_\ell}\frac{\partial \overline{u_i u_j}}{\partial x_\ell} \qquad (25)$$

Hanjalic and Launder[12] neglected the first term on the right-hand side of Eq. (24) based on their experimental measurements of axisymmetric flow in a plane channel.[13] Furthermore, upon neglecting the convective transport of Eq. (24), the following algebraic equation was obtained.

$$\overline{u_i u_j u_k} = -0.08\, C_3 \frac{k}{\varepsilon}\left[\overline{u_i u_\ell}\frac{\partial \overline{u_j u_k}}{\partial x_\ell} + \overline{u_j u_\ell}\frac{\partial \overline{u_k u_i}}{\partial x_\ell} + \overline{u_k u_\ell}\frac{\partial \overline{u_i u_j}}{\partial x_\ell}\right] \qquad (26)$$

Shir[14] proposed the following expression

$$\overline{u_i u_j u_k} = - 0.04\ C_3\ \frac{k^2}{\varepsilon}\ \frac{\partial \overline{u_i u_j}}{\partial x_k} \tag{27}$$

Cormack et al.[15] obtained algebraic expressions by approximating the experimentally determined profiles for $\overline{u_i u_j}$, ε and $\overline{u_i u_j u_k}$ with a polynomial with coefficients chosen to give a least-square fit to the data and discretized the cross-stream coordinate in each flow into p grid intervals by using the most general model for the triple velocity correlation tensor as generated using the asymptotic approach of Lumley and Khajeh Nouri.[7] The model they obtained is as follows:

$$\begin{aligned}\overline{u_i u_j u_k} = \frac{4k^2}{\varepsilon} C_3 \ \{2\alpha_1 (\delta_{ij}\ \delta_{k\ell} + \delta_{ik}\ \delta_{j\ell} + \delta_{kj}\ \delta_{i\ell})\ \frac{\partial k}{\partial x_\ell} \\ + \alpha_5 (\frac{\partial a_{ik}}{\partial x_j} + \frac{\partial a_{ij}}{\partial x_k} + \frac{\partial a_{kj}}{\partial x_i})\} + \frac{2k}{\varepsilon} \{2\alpha_7 (\delta_{ik} a_{j\ell} + \delta_{ij} a_{k\ell} \\ + \delta_{jk} a_{i\ell})\ \frac{\partial k}{\partial x_\ell} + \alpha_{12} (a_{ik} \frac{\partial a_{j\ell}}{\partial x_\ell} + a_{ij} \frac{\partial a_{k\ell}}{\partial x_\ell} + a_{kj} \frac{\partial a_{i\ell}}{\partial x_\ell})\}\end{aligned} \tag{28}$$

where

$$a_{ij} = \overline{u_i u_j} - \frac{2}{3} k \delta_{ij} \tag{29}$$

Out of the twenty parameters, α_i, that they had started out with, they were able to determine and optimize the most significant ones as being α_1, α_5, α_7 and α_{12}. The values of these parameters have been recommended for various kinds of flows along with the universal value applicable to most of the flows.

$$\alpha_1 = -\ 8.14 \times 10^{-3}$$

$$\alpha_5 = -\ 1.72 \times 10^{-2}$$

$$\alpha_7 = -\ 4.80 \times 10^{-2} \qquad (30)$$

$$\alpha_{12} = -\ 0.102$$

In the original modes of Eqs. (25)-(28), the coefficient C_3 was chosen to be 1, but the best values for C_3 were investigated for the reattaching shear flows by comparison with experimental data. The recommended values are given in Sec. 4.3.

3. NUMERICAL MODEL

3.1 Numerical Method

The solution method of the transport equations described in the preceding section is the same finite volume method as that employed in TEACH Code,[16] while the differencing scheme is the modified hybrid scheme of Amano[17] in which the combined mode of convection and diffusion is derived by expanding the analytical one-dimensional solution up to the fourth-order term. The cell structure for mean-velocity components is the staggered system in which the locations of the mean velocities U and V are a half-cell shifted in x- and y-directions, respectively. All the normal Reynolds stresses ($\overline{u_i^2}$) are evaluated at the scalar node point along with P, k and ε. However, the shear Reynolds stress ($\overline{uv}$) is located at the southwest corner of the scalar cell. This is because the main driving strains for the shear stress are $\partial U/\partial y$ and $\partial V/\partial x$ which can easily be evaluated without any interpolations (Fig. 1).

3.2 Boundary Conditions

There are three different types of boundary conditions to be specified for the computation of a flow in the channel as shown in Fig. 2: inlet, outlet, and wall boundary conditions.

At the inlet all the quantities are specified according to the fully developed condition. At the outlet a continuative flow condition is applied where gradients of flow properties in the flow direction are zero (Neumann conditions), i.e., $\partial\phi/\partial x = 0$, where $\phi = U_i$, k, ε, $\overline{u_i u_j}$, etc. This outlet is located about 80-120H downstream from the step so that its influence on the main flow region is negligibly small.

At the wall boundaries the velocities and turbulence quantities must be specified functionally according to the drag law or the law of the wall. For example, the tangential velocity can be expressed in terms of wall shear stress as a functional expression of the boundary condition coupled with the no-slip condition as

$$F = \tau \delta A \tag{31}$$

where δA = wall area of the cell. The velocity component normal to the wall is simply set as zero. The wall boundary values for k and ε are determined by means of wall functions based on the assumption of a logarithmic near-wall velocity distribution which allows the wall-shear stress to be extracted from the "log law" and the value of velocity parallel to the wall to be computed along the grid line closest to the wall. Near-wall effects on the turbulence structure, associated with the steep velocity variations, are also taken into account by introducing appropriate modifications to the generation and dissipation of the turbulent energy and the energy dissipation rate for the finite volume adjacent to the wall.[17]

The boundary values for the Reynolds stresses are determined as

$$\overline{u^2} = 1.21k$$

$$\overline{v^2} = 0.24k \qquad (32)$$

$$\overline{-uv} = -0.24k + \frac{\nu}{\rho}\frac{dP}{dx}$$

in the wall adjacent numerical cells. These boundary conditions are developed noting the following points: i) the coefficients in the normal stresses represent a consensus of several reported wall flows, and ii) the boundary condition for the shear stress is given by the mean momentum equation. The details of the derivation of Eq. (32) are given in the Appendix.

3.3 Computing Details

Exploratory tests were made for different mesh sizes to investigate an optimum grid-independent state. Figure 3 represents a length of reattachment for different grid expansion factors in x-direction ranging from 1.01 to 1.05 and for different numbers of grid points in x- and y- directions. The larger value of the expansion factor ϵ_x creates a finer mesh in the recirculating region while it results in a coarser mesh size in the downstream region far from the step. As shown in the figure, the variation in the reattachment length does not exceed 2% between the medium value of 1.03 and the relatively fine value of 1.05. Also, the grid system almost reaches a grid-independent state around 40 grid points for both x- and y- directions. For most of the computations a 42 x 42 grid system is used with an expansion factor of 1.03 in x-direction. However, it should be emphasized that the above mentioned test is made only for a prediction of a reattachment length. At this stage we

simply carried out most of the computations based on this test leaving the refinement of the grids for the Reynolds stresses or other turbulence quantities to the next progress report.

In the computation of the Reynolds-stress equations (7), initial stress values have to be specified properly so as not to cause numerical divergence since the system of equations is relatively unstable. This instability is mainly due to an explicit form of the Reynolds-stress equations which contains Reynolds stresses in most of the terms on the right-hand side. Thus a new value of $\overline{u_i u_j}$ is computed by inserting previously computed $\overline{u_i u_j}$ iteratively until it converges. This instability problem was overcome by employing a three-pass procedure, that is, the computation was initially started with the standard $k \sim \varepsilon$ model. The Boussinesq viscosity model of the Reynolds stresses was invoked when the maximum residual source of the mass and momentum became 5 percent of the total inlet mass or momentum which was attained in about 50 iterations. The transport equations of the Reynolds stresses were brought in when this residual source became 3 percent which took another 20 iterations. Complete convergence was assumed to have been attained when the relative maximum residual source of the Reynolds stresses was less than 1.7×10^{-3} which required typically another 320 iterations with a total CPU time of about 50 minutes on a UNIVAC 1100 computer.

4. RESULTS AND DISCUSSION

4.1 Mean Velocity Profiles

The flow in the channel shown in Fig. 2 was computed by using the models described in the preceding section, and the results were compared with available experimental data.

Figure 4 shows the velocity profiles at several different locations along the flow-stream for the channel step ratio $Y_o/H = 3$ and for $Re_\theta = 5000$. Both the computations by the $k \sim \varepsilon$ model and the RSM were compared with the experimental data of Seegmiller and Driver[18], at three streamwise positions ($x/H = 2$, 5.56, and 8.63), where the reattachment point was about $x_r/H \simeq 5.0$. Thus, $x/H = 2$ corresponds to the position in the recirculating region, $x/H = 5.56$ to the position near the reattachment point, and $x/H = 8.63$ is the position in the flow redeveloping region. It is observed that agreement between the experimental data and computational results in the recirculating and reattachment regions is not as good as that in the redeveloping region. This is because the numerically predicted reattachment length, $x_r/H = 5$, is somewhat different from that determined by the experiment, $x_r/H = 7$. Moreover, although the difference between the computations by the $k \sim \varepsilon$ model and the RSM is not remarkable, the RSM consistently gives slightly better results.

Figure 5 shows the velocity profiles for the step ratio $Y_o/H = 2$ at three locations: $x/H = 2.67$, 5.33 and 9.78. The location $x/H = 5.33$ is very near the reattachment point since the computed x_r/H is about 5.5. In addition, the computations are compared with the experimental data of Kim et al.[19] where the trend of the prediction is quite similar to that in Fig. 4. However, in this case agreement between experiment and computation in the recirculating region is better than that found near the reattachment point. The disagreement near the reattachment point is because there is a discrepancy in the prediction of the reattachment length between experiment ($x_r/H = 7$) and computation ($x_r/H = 5.5$).

In Figs. 4 and 5 the computations by an algebraic stress model (ASM) made by Sindir[20] are also compared. The best agreement for the recirculating region is predicted by the ASM and for the redeveloping region by the RSM.

As discussed above, the turbulence model is dependent on the location of the flow field. In the recirculating region the RSM provides slightly better predictions near the wall. However, in the shear flow part, the ASM gives the best agreement with measurements. In the reattachment region the RSM shows the slowest velocity recovery performance while at the same time in the redeveloping region it shows the best prediction. Since the behavior of the mean velocity is closely related to the performance of Reynolds stresses, we will next examine the action of normal and shear stresses in the flow region across the streamwise flow.

4.2 Reynolds Stresses

Figures 6 and 7 show, respectively, the normal and shear stress profiles for the channel expansion of $Y_0/H = 3$, which correspond to the velocity profiles in Fig. 4. The experimental data of Seegmiller and Driver[18] are also shown in these figures. The normal stresses increase rapidly with the distance from the bottom wall and reach their maxima at about $y/H = 1.0$ in the recirculating region and at $y/H = 0.5 - 0.7$ in the reattachment and redeveloping regions. The stresses then decrease to very small values at approximately $y/H = 1.3 - 1.5$. It is of interest to note that the y location of the peak moves upwards in the order of the $k \sim \varepsilon$, RSM, and ASM. The level of normal stresses also increases in the same order as the peak location. A similar trend is also observed for the shear stress distributions except that they have negative values.

With regard to the comparison between measurement[18] and computations, the predictions by the ASM seem to be better for the normal stresses while those by the RSM are closer to the experimental data for the shear stresses. The predicted levels of the Reynolds stresses by the $k \sim \varepsilon$ model are always too low.

Observation of these Reynolds stresses indicates that the performance of the Reynolds-stress prediction does not necessarily accord with the computation of the mean velocity profiles which are shown in Fig. 4. At $x/H = 2$, the RSM gives better agreement, but the ASM is superior for normal stresses in the redeveloping region. Generally, we see the success of the Reynolds-stress closure in the prediction of the shear-stress distributions.

4.3 Triple Velocity Products

Computations for the triple velocity products were performed for two sets of flow conditions corresponding to the experimental data of Driver and Seegmiller[21] and Chandrsuda and Bradshaw.[22]

Figures 8, 9 and 10 show the profiles for the normalized triple velocity products $(\overline{uuv} + \overline{vvv})/U_{IN}^3$ as a function of nondimensional distance from the step y/H at three different locations of $x/H = 4.0$, 6.0 and 8.0. The computation was performed using a 42 x 42 mesh with cell expansion factors of 1.03 and 0.98 in the axial and transverse directions, respectively. Triple velocity products were obtained by the four correlations proposed by Daly and Harlow[5], Hanjalic and Launder[12], Shir[14], and Cormack et al.[15], and are compared with the experimental data of Driver and Seegmiller[21] for a backward-facing step with a step ratio, $Y_o/H = 8$.

The models given in Eqs. (25)-(28) were used to compute the triple velocity products after all the converged solutions of the Reynolds stresses were obtained.

All these models for the triple velocity correlations were initially developed to satisfy the conditions of relatively simple types of flow such as free jets, wakes, boundary layers, etc. Therefore it is necessary to modify these models for the present reattaching and recirculating flows. The coefficient, C_3, in Eqs. (25)-(28) was examined in order to determine optimum results of triple velocity products throughout the solution domain.

Upon comparing the coefficients C_3 in these correlations with the experimental data, it was found that the value of C_3 differed by a factor of 1 to 50 among different correlations. The determination of this empirical multiplication factor, C_3, is based upon a simple averaging method wherein the peak maxima and minima are measured and compared with the experimental data and factors were thus obtained.

The factors developed and used are given in Table 1.

Table 1. Factors used in different models

Model	C_3
Shir	53.13
Hanjalic and Launder	6.27
Cormack et al.	5.67
Daly and Harlow	1.06

The general trend prescribed by these correlations is very similar to the experimental data as seen in the Figs. 8, 9 and 10.

Figures 11, 12 and 13 compare the experimental data of Chandrsuda and Bradshaw[22] for a backward-facing step with a step ratio $Y_0/H = 2.5$ with the triple velocity products obtained by the aforementioned four correlations at three different locations of $x/H = 5.4$, 8.4, and 10.3, respectively. These

computations were performed using a 52 x 52 mesh with cell expansion and contraction factors of 1.015 and 0.990 in the axial and transverse directions, respectively. The computational technique was similar to the one used to compute the data for $Y_o/H \sim 8$ except for the fact that the convergence was assumed to have been completed when the maximum residual source was 1.5 percent (which is independent of the source term for Reynolds stresses), which took about 620 iterations total. In this computation about 200 iterations were performed for solution of the transport equations of the Reynolds stresses. Total CPU time on a UNIVAC 1100 computer was about 90 minutes.

Figure 11 compares the variation of $\overline{vvv}/U_{IN}^3$ as a function of y/H at the location x/H = 5.4 with different correlations and the experimental data. Figure 12 compares the variation of $\overline{uuv}/U_{IN}^3$ as a function of y/H at the location x/H = 8.4, and Fig. 13 compares the variation of $\overline{uuv}/U_{IN}^3$ at the location x/H = 10.3. There is generally good agreement between the results of the correlations and the experimental data as seen in these figures.

It is rather premature to discuss the relative merits and demerits of each correlation of triple velocity products at this stage. However, it has been seen that most of the correlations presented here may be improved with only minor modifications.

5. SUMMARIZING REMARKS

Through the first six month period, a hybrid model of the Reynolds-stress closure was developed. This model was tested for various sizes of step flow, and the computed Reynolds-stress behavior was compared with experimental data as well as with other simpler turbulence models such as the algebraic stress

model and the standard $k \sim \varepsilon$ model. Although the results are not drastically improved with the RSM, it is shown that overall agreement with experimentally measured values for both the mean velocity and the Reynolds stresses is better than other models. Moreover, the application of the RSM to flows in geometrically more complicated shapes is promising. It is also noted that the $k \sim \varepsilon$ model or the ASM cannot be used for such complex flow predictions due to the fact that the $k \sim \varepsilon$ model is limited only to a quasi-isotropic flow and the ASM is applicable only when the convective effect of the Reynolds stress is not important.

Secondly, the third-order closure model was reviewed and transport equations for the triple velocity correlation were developed and implemented in a numerical code to evaluate the behavior of the triple velocity products in various regions of the flow field including recirculating, reattaching, and redeveloping flow domains. These four existing models of algebraic equations for the triple velocity products were also employed in a program and a modification of the empirical coefficients was made to improve the prediction for the reattaching shear flows.

Probably the most significant fact the investigators have learned through this project is that both convection and diffusion effects of the triple velocity products become very important in the reattaching shear layer which has been ignored by most of the researchers. It is our aim to pursue the effects of these rates in the third-order closure model. In the next stage of this project, the transport model of the third-order closure will be implemented and tested for universal usage.

6. WORK IN PROGRESS

6.1 QUICK Method

Although all the computations made in this report are done by using the modified hybrid scheme specified in Sec. 3.1, the authors are seeking a better discretization method for computing the transport equations used in this project.

When convection of a transport equation does not predominate over diffusion, the exclusive use of central differencing in space undoubtedly offers a satisfactory compromise between the requirements of accuracy and computational economy. However, when convection is dominant, central differencing for convection results in instability. To avoid this instability, a false diffusion is frequently brought in at an expense of accuracy.

The reduction of false diffusion in the computation of steady-state recirculating flows at no significant loss of computational economy has been one of the objects of this project. Some of the schemes proposed by several researchers have been reviewed. The "skew-upwind-differencing scheme" of Raithby[23] yields a certain amount of reduction in skewness error by partially simulating an upwind discretization in a stream-line coordinate system. By using Raithby's method, skewness errors are totaly absent although it is only first-order accurate. The method of Leonard[24] is of a more fundamental nature, designed to eliminate false diffusion altogether by using a convective manner, i.e., quadratic, upstream-weighted interpolation for the convection terms (QUICK).

The original work of the QUICK method demonstrated by Leonard was for one-dimensional and for uniform-grid system only. Thus this method needs to

be tailored for more general two-dimensional and non uniform grid systems. The procedure for this is given as follows.

Consider the problem of approximating ϕ_w in Fig. 14. Depending on the sign of U_w either points WW, W and P or points W, P and E are used to fit a quadratic curve for interpolating the value of ϕ at w. A length δ_3 is now defined as the distance from the west face to either the WW-point or E-point depending on the direction of U_w. It can be written as

$$\delta_3 = \begin{cases} \Delta x_{PE} + \delta_2 & U_w < 0 \\ -(\Delta x_{WW-W} + \delta_1) & U_w > 0 \end{cases} \tag{33}$$

A quadratic fit then yields for ϕ_w as

$$\phi_w = \frac{B_1}{B}\phi_w - \frac{B_2}{B}\phi_p + \frac{B_3}{B}\phi_* \tag{34}$$

where

$$\phi_* = \begin{cases} \phi_{WW} & U_w > 0 \\ \phi_E & U_w < 0 \end{cases} \tag{35}$$

and

$$\begin{aligned} B_1 &= \delta_2\delta_3(\delta_2 - \delta_3) \\ B_2 &= \delta_1\delta_3(\delta_1 + \delta_3) \\ B_3 &= \delta_1\delta_2(\delta_1 + \delta_2) \\ B &= B_1 - B_2 + B_3 \end{aligned} \tag{36}$$

The above formulations are implemented for a two-dimensional system.

So far the implementation of QUICK is done only for the momentum equations--it is still being tested for the rest of the equations. Therefore it seems to be premature to conclude any advantages and disadvantages connected with its use. However, we feel that there would be only small differences in the results of the third-order closure model no matter which system is employed. As is noted in most of the transport equations, generations and dissipations are mainly evaluated through the source terms of the discretization equations not through the convection-diffusion discretization.

6.2 Consolidation of the RSM

The work described in the preceding sections is not a complete model of the full Reynolds-stress equations. The diffusion terms of the momentum (Eq. (2)) and the dissipation equations (Eq. (5)) still contain the Boussinesq viscosity approximation simply because the solutions become numerically unstable when we employ the Reynolds stresses in these diffusion terms. It was also mentioned that the third-order closure was employed only after all the converged solutions for the Reynolds stresses had been obtained. The following briefly summarizes the work currently being conducted to accomplish the coding of the full Reynolds-stress model.

1) Diffusion Rate of Momentum Equations.

The form of Eq. (2) was converted into the following form:

$$\frac{\partial}{\partial x_j}(\rho U_i U_j) = -\frac{\partial P}{\partial x_i} + \frac{\partial}{\partial x_j}\left[\mu\left(\frac{\partial U_i}{\partial x_j} + \frac{\partial U_j}{\partial x_i}\right) - \frac{\overline{\rho u_i u_j}}{\partial U_i/\partial x_j}\frac{\partial U_i}{\partial x_j}\right] \tag{37}$$

Equation (37) can be cast into the standard form as

$$\frac{\partial}{\partial x_j}(\rho U_i U_j) = -\frac{\partial p}{\partial x_i} + \frac{\partial}{\partial x_j}\left[\left(\mu - \frac{\rho\overline{u_i u_j}}{\partial U_i/\partial x_j}\right)\frac{\partial U_i}{\partial x_j}\right] + \frac{\partial}{\partial x_j}\left(\mu \frac{\partial U_j}{\partial x_i}\right) \tag{38}$$

In solving Eq. (38) numerically, the first and the third terms on the right-hand side are evaluated in the source term of the discretization equation, whereas the second term is treated as a diffusion term where the effective viscosity becomes

$$\mu_{eff} = \mu - \frac{\rho\overline{u_i u_j}}{\partial U_i/\partial x_j} \tag{39}$$

This treatment is found to cause less instability and the convergence process is improved.

2) Diffusion Rate of ε-Equation.

The dissipation equation (Eq. (5)) which is used to solve the RSM, is a second-order model except for the diffusion term which is again evaluated by using the Boussinesq viscosity model. The complete second-order ε-equation can be obtained by replacing the last term in Eq. (5) by the following

$$D(\varepsilon) = \frac{\partial}{\partial x_j}\left[\left(\mu + C_\varepsilon \frac{\rho k}{\varepsilon}\overline{u_i u_j}\right)\frac{\partial \varepsilon}{\partial x_i}\right] \tag{40}$$

The mechanism and significance of both primary and secondary diffusion terms are now being investigated.

3) Merging the Triple Velocity Products in the RSM.

As mentioned earlier in this report, the behavior of the third-order tensor has a strong effect particularly near the reattaching flow region. This will considerably influence the diffusive action of the RSM. This is the main object of the modeling of the third-order closure.

For the same reason as stated in case (1) of this section, the form of Eq. (11) is recommended to be modified to a formal diffusion term such as those given by Eq. (18). Consequently, Eq. (11) was transformed into the following

$$D_{ij} = -\frac{\partial}{\partial x_k}\left[\frac{\overline{u_i u_j u_k}}{\partial(\overline{u_i u_j})/\partial x_m}\frac{\partial \overline{u_i u_j}}{\partial x_m}\right] \tag{41}$$

The computation of Eq. (41) is now being undertaken in parallel with the development of the third-order closure model.

7. APPENDIX

7.1 Near-Wall Values for Reynolds Stresses

At the wall the boundary conditions for the Reynolds stresses are determined as follows. First, the boundary condition on $\overline{uv}$ is given by the mean momentum equation (Eq. (2)). Near the wall where convection of the momentum is negligibly small, Eq. (2) yields the following form.

$$0 = -\frac{dP}{dx} + \frac{d}{dy}(\tau_w - \rho\overline{uv}) \tag{A.1}$$

It is also known from the Law of the Wall that the wall shear stress may be given as

$$U_\tau^2 = \tau_w/\rho \tag{A.2}$$

Thus, by integrating Eq. (A.1) and after substituting Eq. (A.2), we obtain the following.

$$-\overline{uv} = -U_\tau^2 + \frac{y}{\rho}\left(\frac{dP}{dx}\right) \tag{A.3}$$

The determination of the normal components of the Reynolds stresses is based on an observation of experimental data. A consensus of several of the most thoroughly documented wall flows [25-28] is represented as

$$\begin{aligned} \overline{u^2} &= 4.5\, U_\tau^2 \\ \overline{v^2} &= 1.0\, U_\tau^2 \\ \overline{w^2} &= 2.0\, U_\tau^2 \end{aligned} \tag{A.4}$$

By using the correlation of the turbulence energy, k, and the friction velocity, U_τ, in the wall proximity region,

$$k = 3.7\ U_\tau^2 \tag{A.5}$$

the values of Eqs. (A.3) and (A.4) become

$$\begin{aligned} -\overline{uv} &= -0.24k + \frac{\nu}{\rho}\frac{dP}{dx} \\ -\overline{u^2} &= 1.21k \\ -\overline{v^2} &= 0.24k \\ -\overline{w^2} &= 0.55k \end{aligned} \tag{A.6}$$

It should be noted that the boundary condition given by Eq. (A.6) satisfies the definition of k, i.e.,

$$k = (\overline{u^2} + \overline{v^2} + \overline{w^2})/2 \tag{A.7}$$

8. REFERENCES

1. Bradshaw, P. and Wong, F. Y. F., "The Reattachment and Relaxation of a Turbulent Shear Layer," Journal of Fluid Mechanics, Vol. 52, Part 1, 1972, pp. 113-135.

2. Smyth, R., "Turbulent Flow Over a Plane Symmetric Sudden Expansion," Journal of Fluids Engineering, Vol. 101, No. 3, 1979, pp. 348-353.

3. Eaton, J. K. and Johnston, J. P., "An Evaluation of Data for the Backward-Facing Step Flow," Stanford Conferences on Complex Turbulent Flows, 1980.

4. Rotta, J. C., "Statistische Theorie Nichthomogener Turbulenz," Z. Phys., Vol. 129, 1951, p. 547.

5. Daly, B. J. and Harlow, F. H., "Transport Equations of Turbulence," Physics of Fluids, Vol. 13, No. 11, 1970, pp. 2634-2649.

6. Naot, D., Shavit, A. and Wolfshtein, M., "Two-point Correlation Model and the Redistribution of Reynolds Stress," Physics of Fluids, Vol. 16, No. 6, June 1973, pp. 738-743.

7. Lumley, J. L. and Khajeh Nouri, B., "Computational Modeling of Turbulent Transport," Advances in Geophysics, Vol. 18A, 1974, pp. 169-192.

8. Launder, B. E., Reece, G. J. and Rodi, W., "Progress in the Development of a Reynolds-stress Turbulence Closure," Journal of Fluid Mechanics, Vol. 68, 1975, pp. 537-566.

9. Rodi, W., "The Prediction of Free Boundary Layers by Use of a Two-Equation Model of Turbulence," Ph.D. Thesis, University of London, Dec. 1972.

10. Amano, R. S. and Goel, P., "A Numerical Study of a Separating and Reattaching Flow by Using Reynolds-stress Turbulence Closure," Numerical Heat Transfer, Vol. 7, No. 3, 1984, pp. 343-357.

11. Millionshtchikov, M. D., "On the Theory of Homogeneous Isotropic Turbulence," C. R. Acad. Sci. S.S.S.R., Vol. 32, 1941, pp. 615-619.

12. Hanjalic, K. and Launder, B. E., "A Reynolds Stress Model of Turbulence and Its Application to Thin Shear Flows," Journal of Fluid Mechanics, Vol. 52, Part 4, 1972, pp. 609-638.

13. Hanjalic, K. and Launder, B. E., "Fully Developed Asymmetric Flow in a Plane Channel," Journal of Fluid Mechanics, Vol. 51, Part 2, 1972, pp. 301-335.

14. Shir, C. C., "A Preliminary Numerical Study of Atmospheric Turbulent Flows in the Idealized Planetary Boundary Layer," Journal of Atmospheric Science, Vol. 30, 1973, pp. 1327.

15. Cormack, D. E., Leal, L. G. and Seinfeld, J. H., "An Evaluation of Mean Reynolds Stress Turbulence Models: The Triple Velocity Correlation," Transactions of the ASME, Journal of Fluids Engineering, Vol. 100, March 1978, pp. 47-54.

16. Gosman, A. D. and Ideriah, F. J. K., "TEACH-T: A General Computer Program for Two-Dimensional, Turbulent, Recirculating Flows," Mechanical Engineering Department Report, June 1976, Imperial College, London.

17. Amano, R. S., "Development of Turbulent Near-Wall Model and Its Application to Separated and Reattached Flows," Numerical Heat Transfer, Vol. 7, No. 1, 1984, pp. 59-75.

18. Seegmiller, H. L. and Driver, D. M., Private Communications, 1984.

19. Kim, J., Kline, S. J. and Johnston, J. P., "Investigation of Separation and Reattachment of a Turbulent Shear Layer: Flow Over a Backward Facing Step," Report MD-37, Thermosciences Division, Department of Mechanical Engineering, Stanford University, 1978.

20. Sindir, M. M., "Effects of Expansion Ratio on the Calculation of Parallel-Walled Backward-Facing Step Flows: Comparison of Four Models of Turbulence," ASME Paper 83-FE-10, 1983.

21. Driver, D. M. and Seegmiller, H. L., "Features of a Reattaching Turbulent Shear Layer Subject to an Adverse Pressure Gradient," AIAA Paper 82-1029, 1982.

22. Chandrsuda, C. and Bradshaw, P., "Turbulence Structure of a Reattaching Mixing Layer," Journal of Fluid Mechanics, Vol. 110, 1981, pp. 171-194.

23. Raithby, G. D., "Skew Upwind Differencing Schemes for Problems Involving Fluid Flow," Computer Methods in Applied Mechanics and Engineering, Vol. 9, 1976, p. 153.

24. Leonard, B. P., "A Stable and Accurate Convective Modelling Procedure Based on Quadratic Upstream Interpolation," Computer Methods in Applied Mechanics and Engineering, Vol. 19, 1979, pp. 59-98.

25. Laufer, J., "Investigation of Turbulent Flow in a Two-Dimensional Channel," NACA Report, No. 1053, 1951.

26. Klebanoff, P. S., "Characteristics of Turbulence in a Boundary Layer with Zero Pressure Gradient," NACA Report, No. 1247, 1955.

27. Chevray, R. and Kovasznay, L. S. G., "Turbulence Measurements in the Wake of a Thin Flat Plate," AIAA Journal, Vol. 7, 1969, p. 1641.

28. Champagne, F. H., Harris, V. G. and Corrsin, S., "Experiments on Nearly Homogeneous Shear Flow," Journal of Fluid Mechanics, Vol. 41, 1970, p. 81.

9. FIGURES

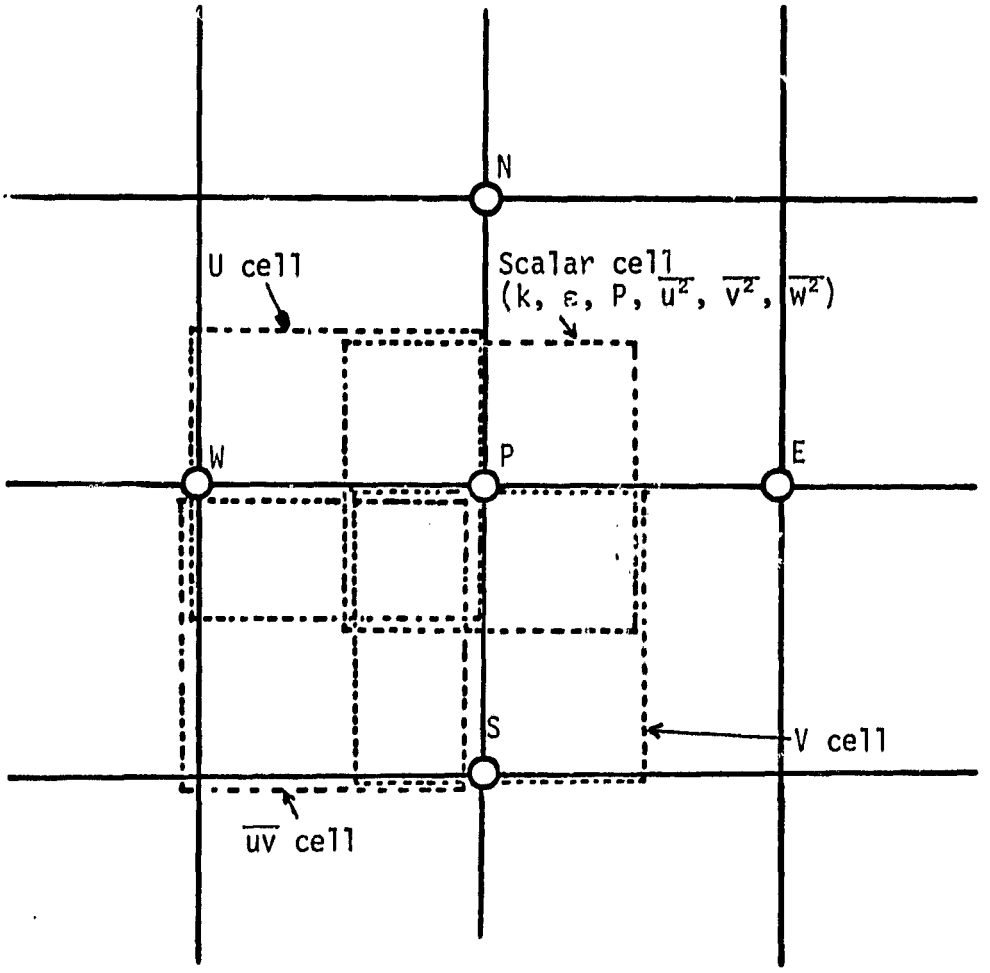

Figure 1 Cell structure.

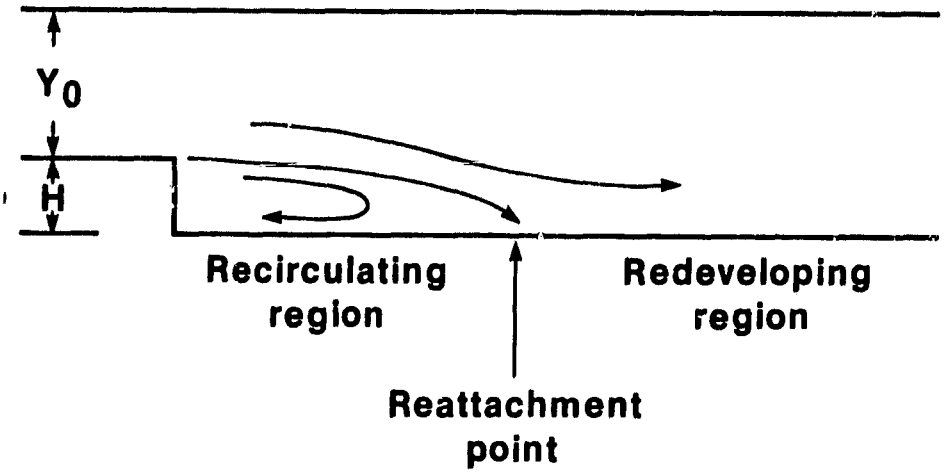

Figure 2 Flow domain.

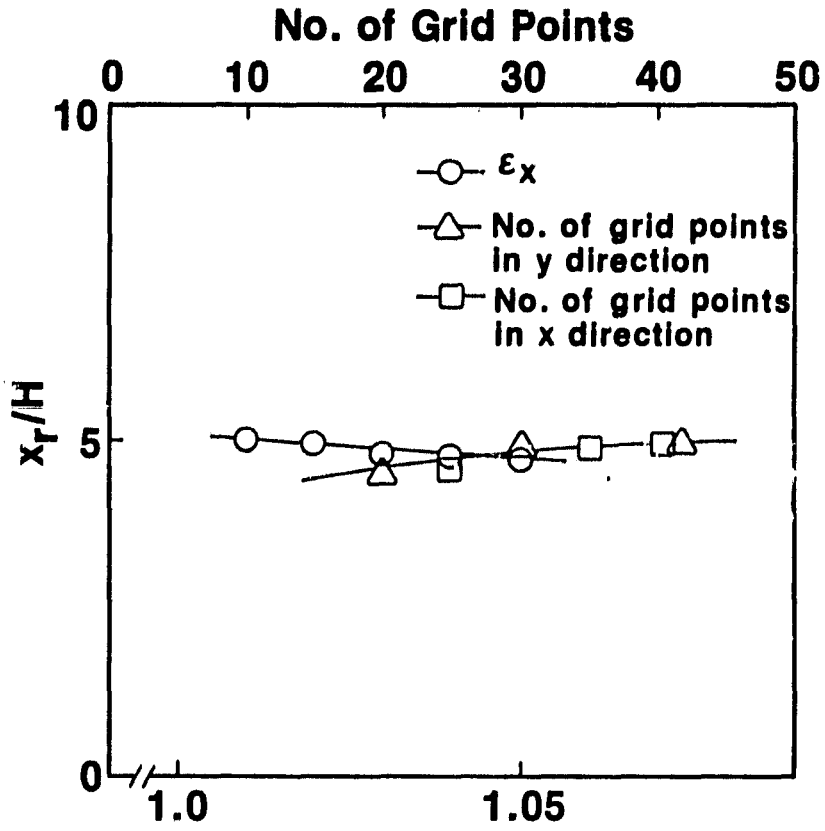

Figure 3 Reattachment length for different grid size.

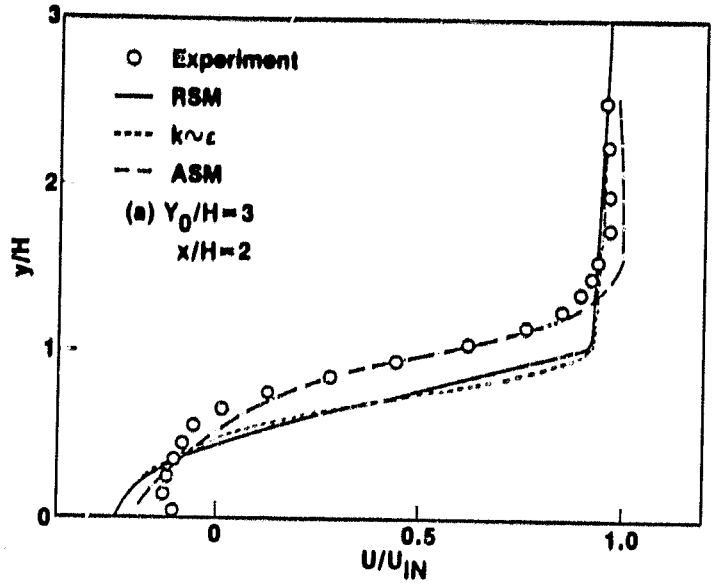

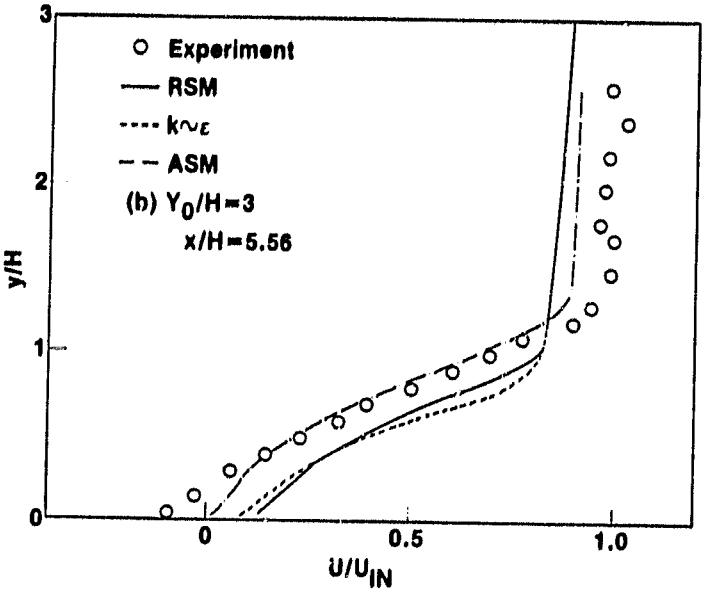

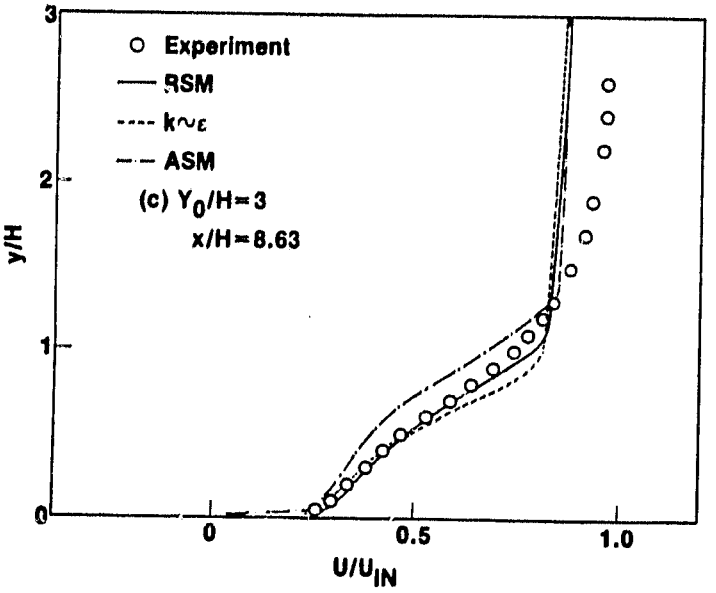

Figure 4 . Mean streamwise velocity profile.

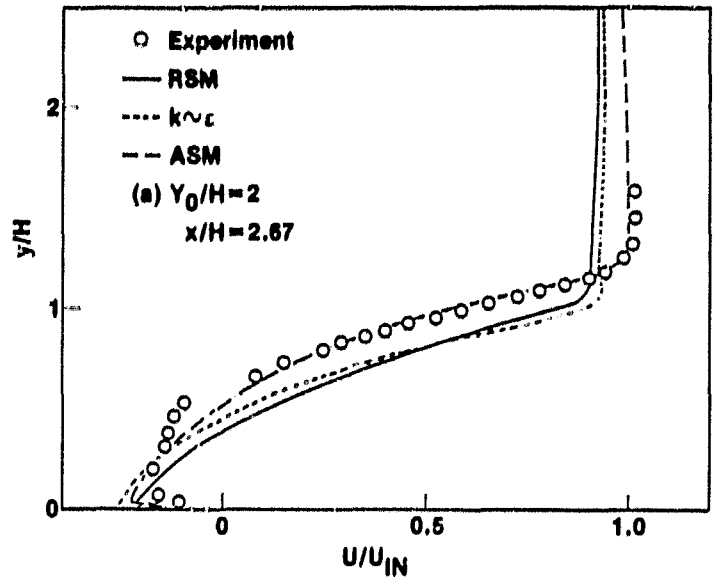

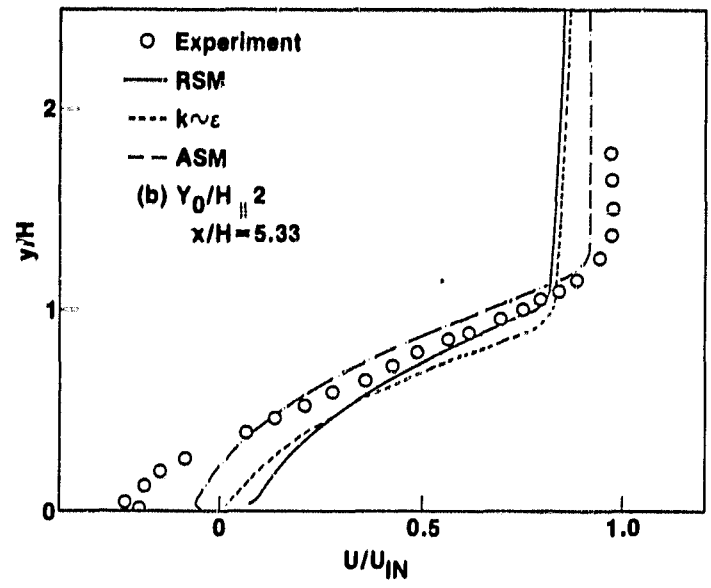

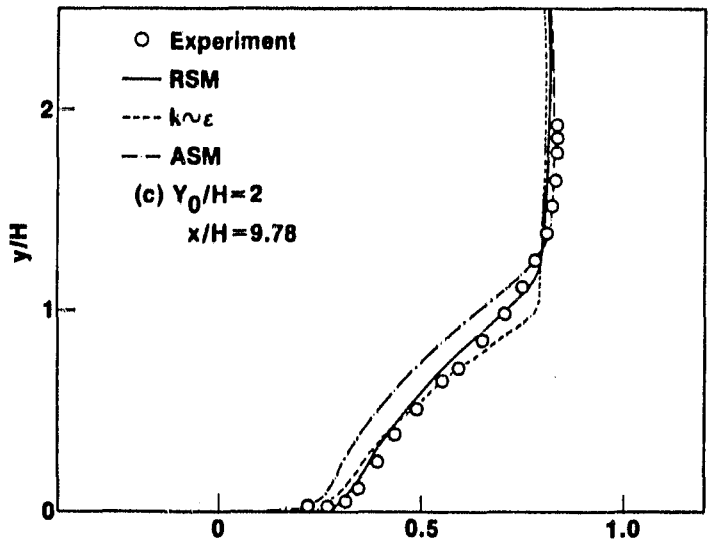

Figure 5 Mean streamwise velocity profile.

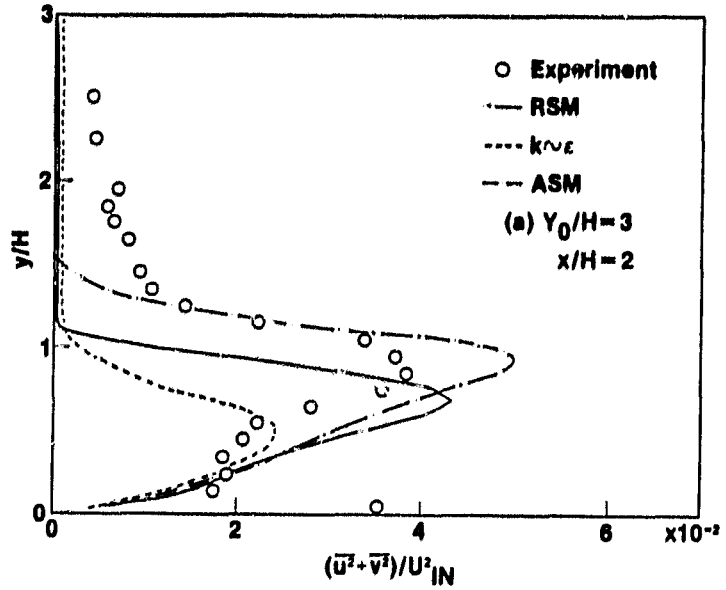

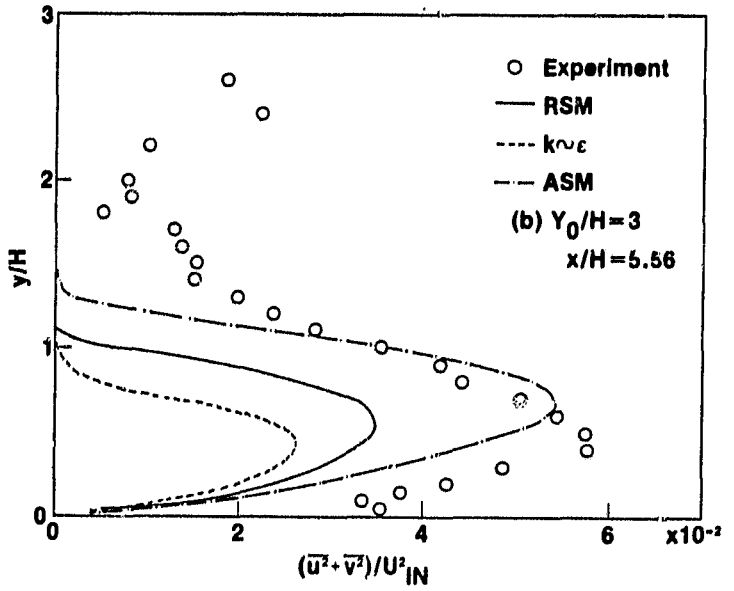

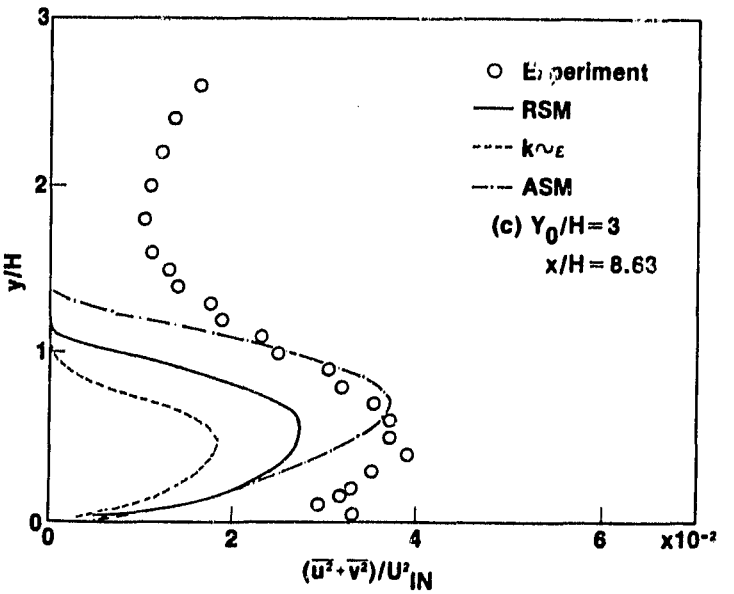

Figure 6 Reynolds normal stress profile.

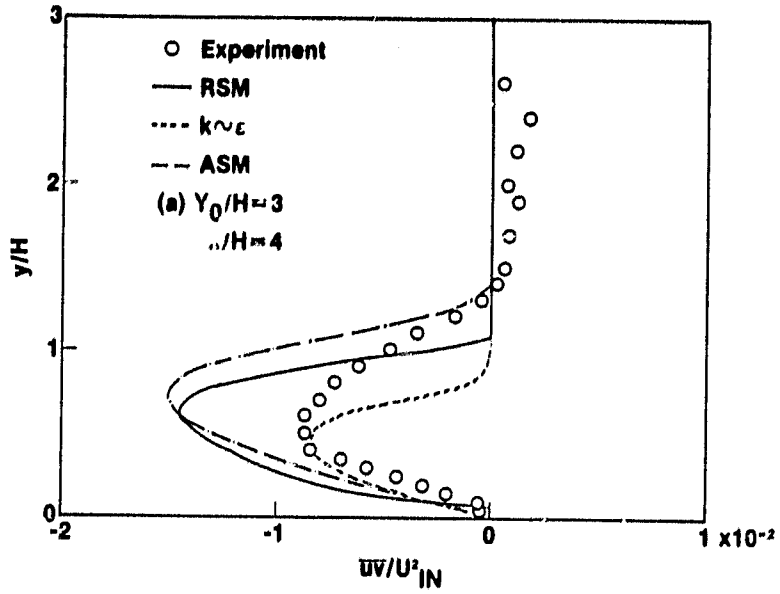

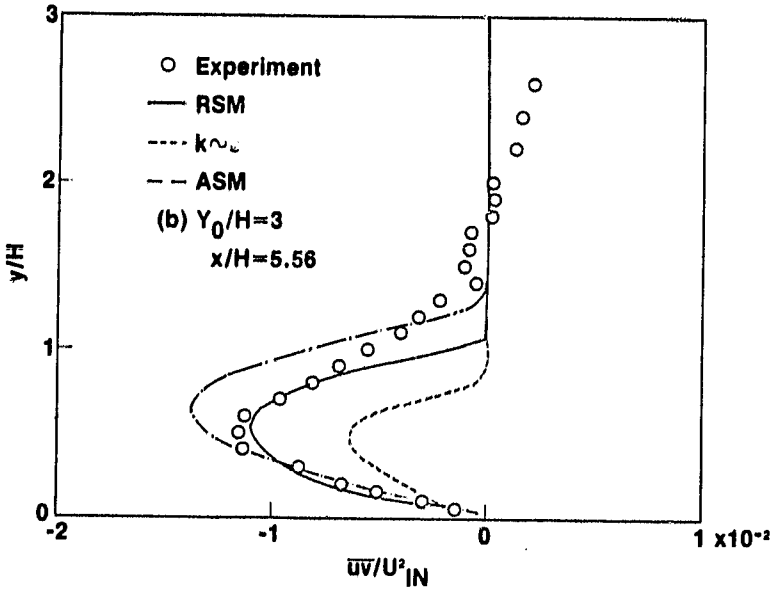

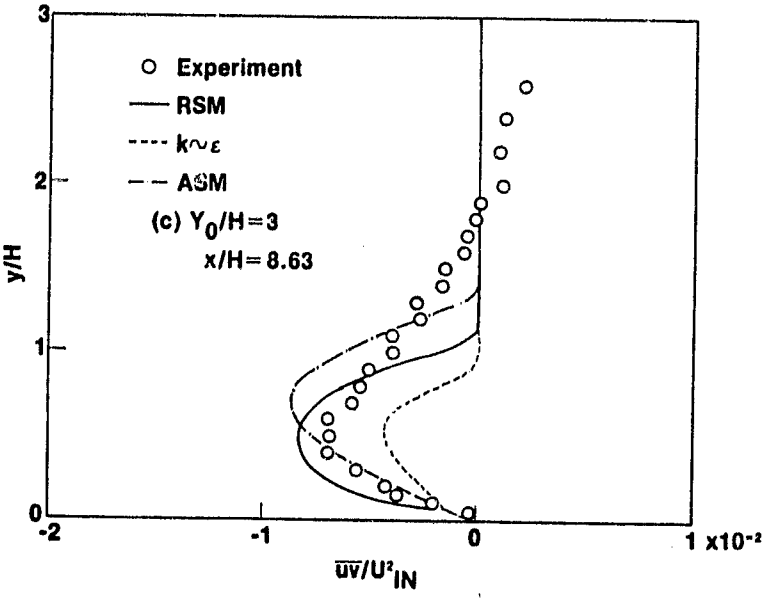

Figure 7 Reynolds shear stress profile.

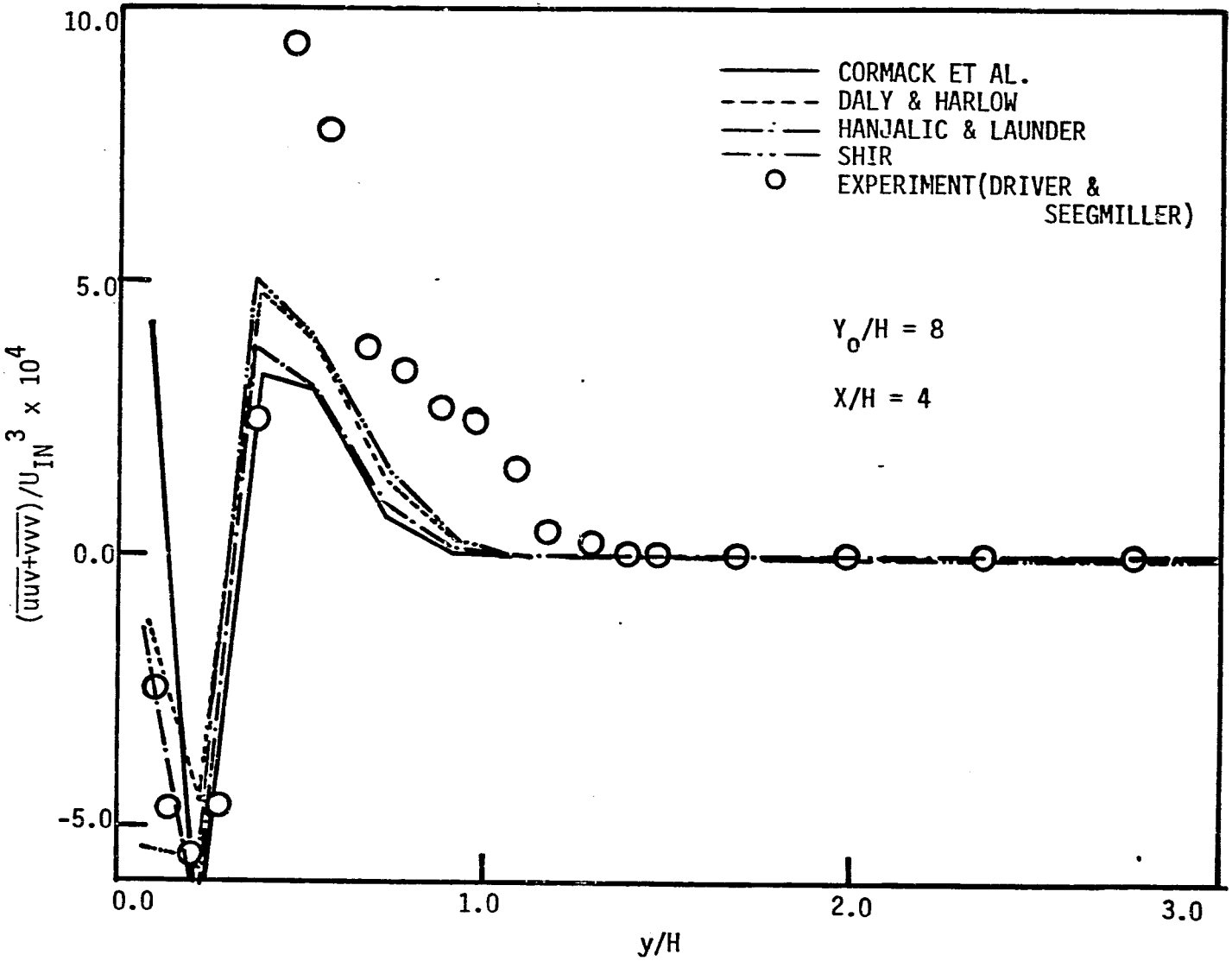

Figure 8 Triple velocity products at x/H = 4.
(comparison with experiment of Driver and Seegmiller)

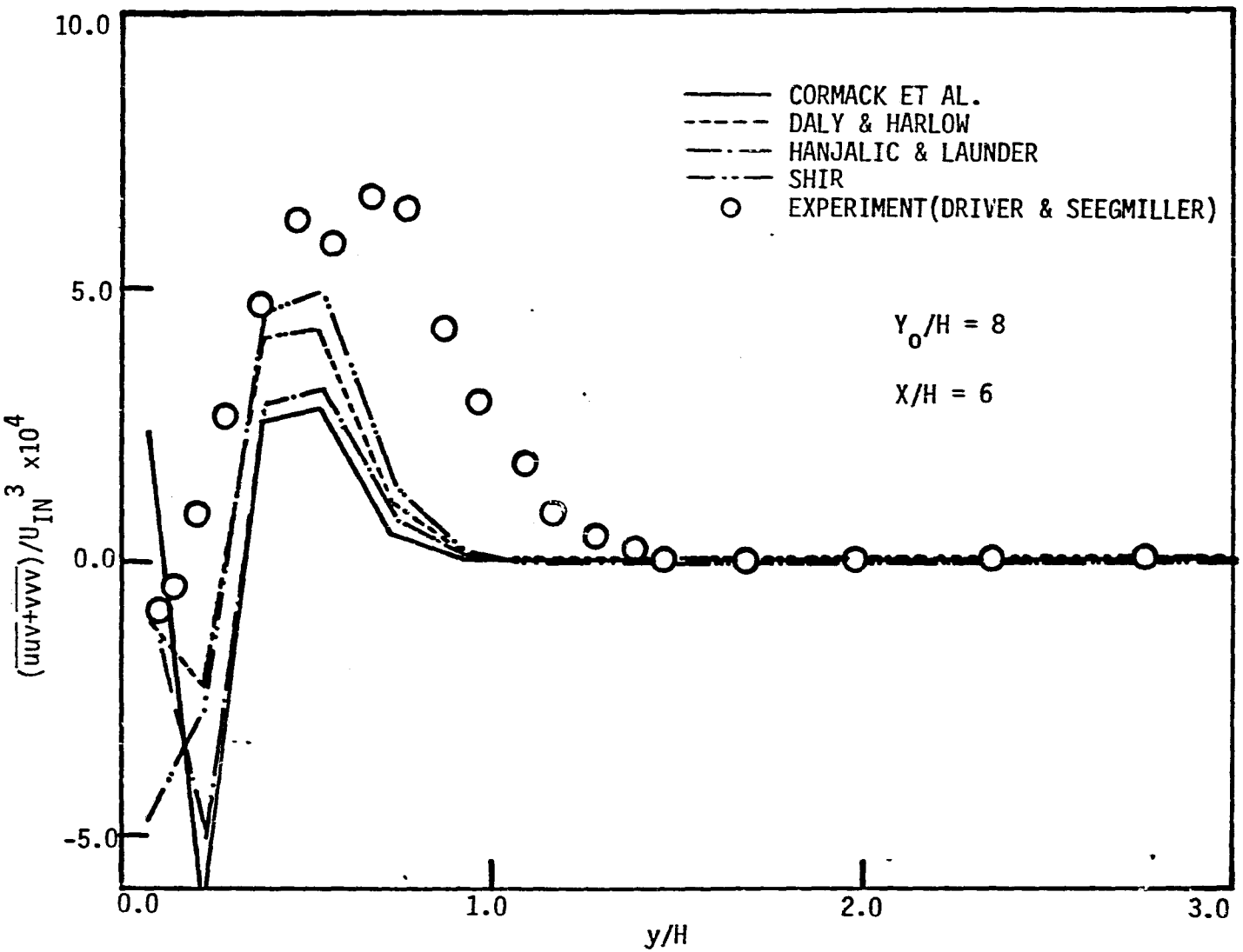

Figure 9 Triple velocity products at x/H = 6.
(comparison with experiment of Driver and Seegmiller)

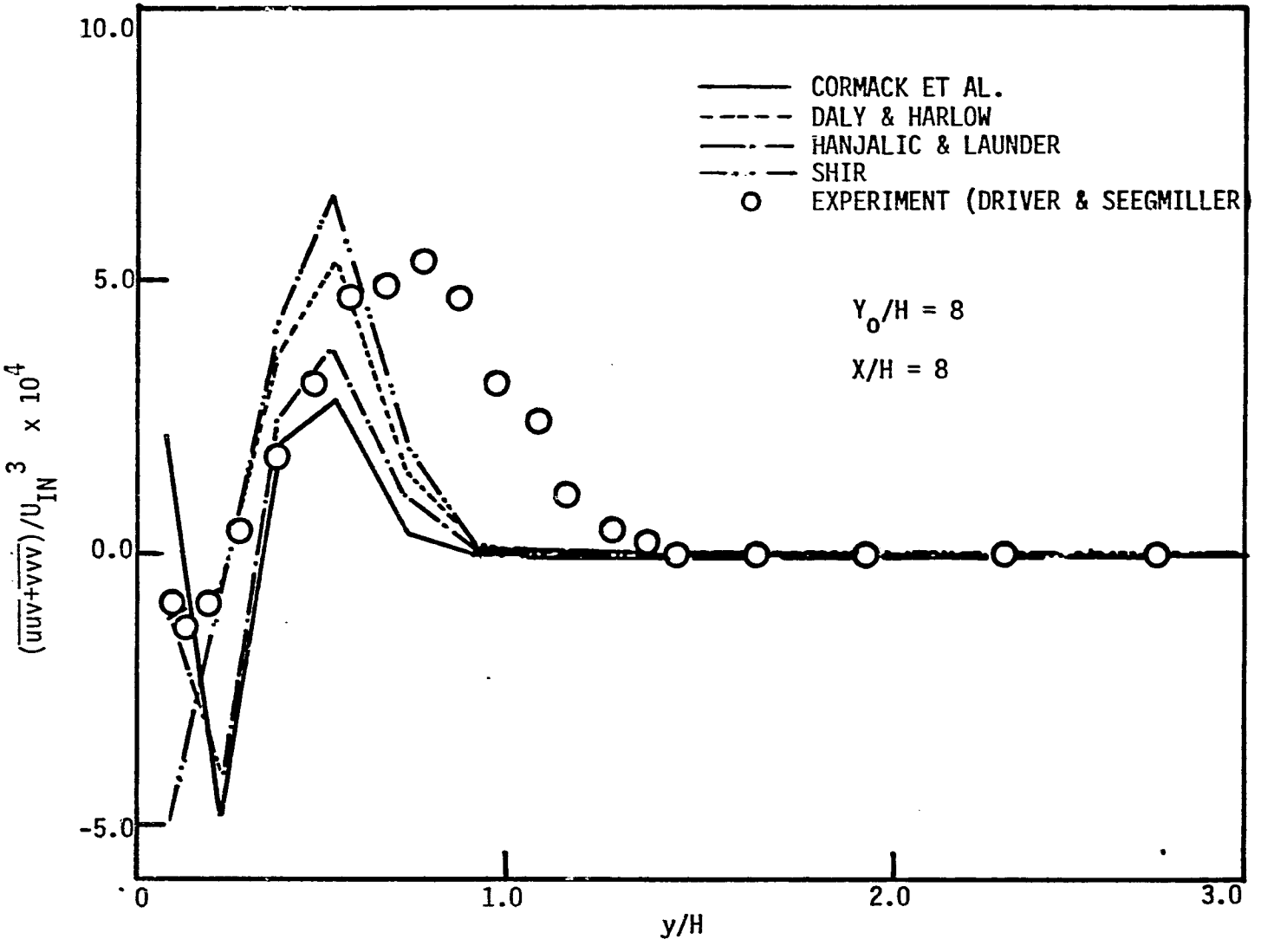

Figure 10 Triple velocity products at x/H = 8.
(comparison with experiment of Driver and Seegmiller)

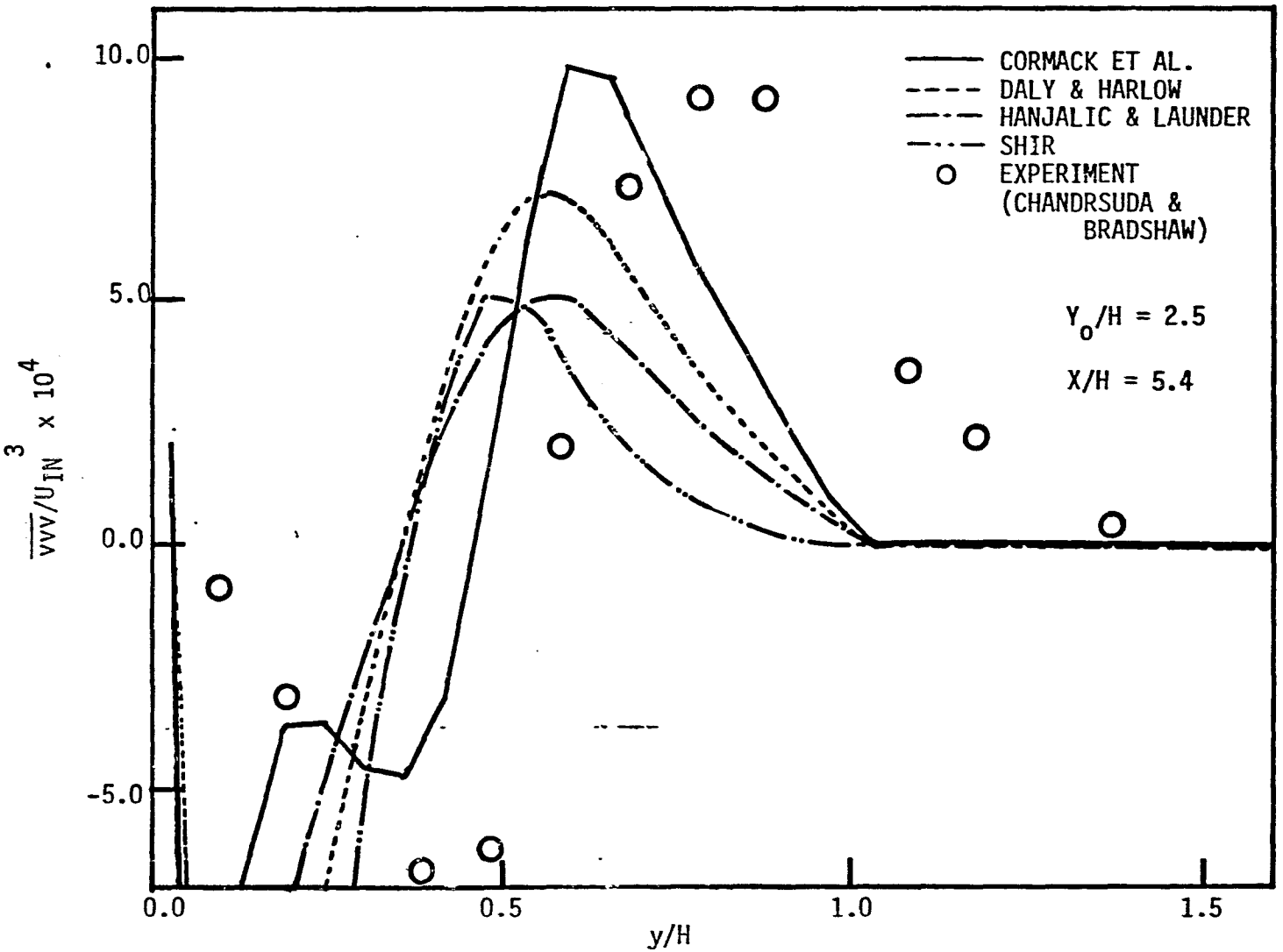

Figure 11 Triple velocity products at x/H = 5.4.
(comparison with experiment of Chandrsuda and Bradshaw)

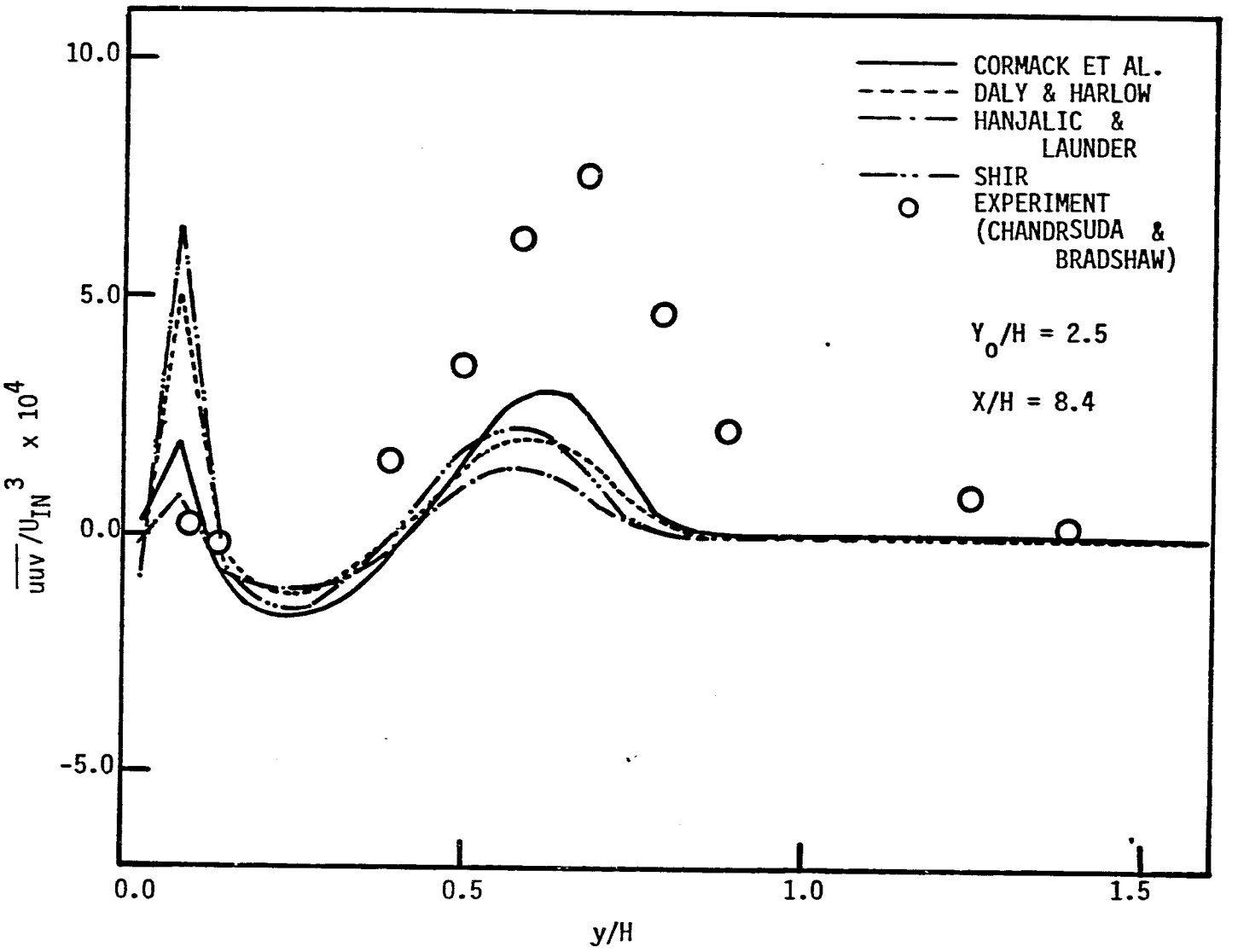

Figure 12 Triple velocity products at x/H = 8.4.
(comparison with experiment of Chandrsuda and Bradshaw)

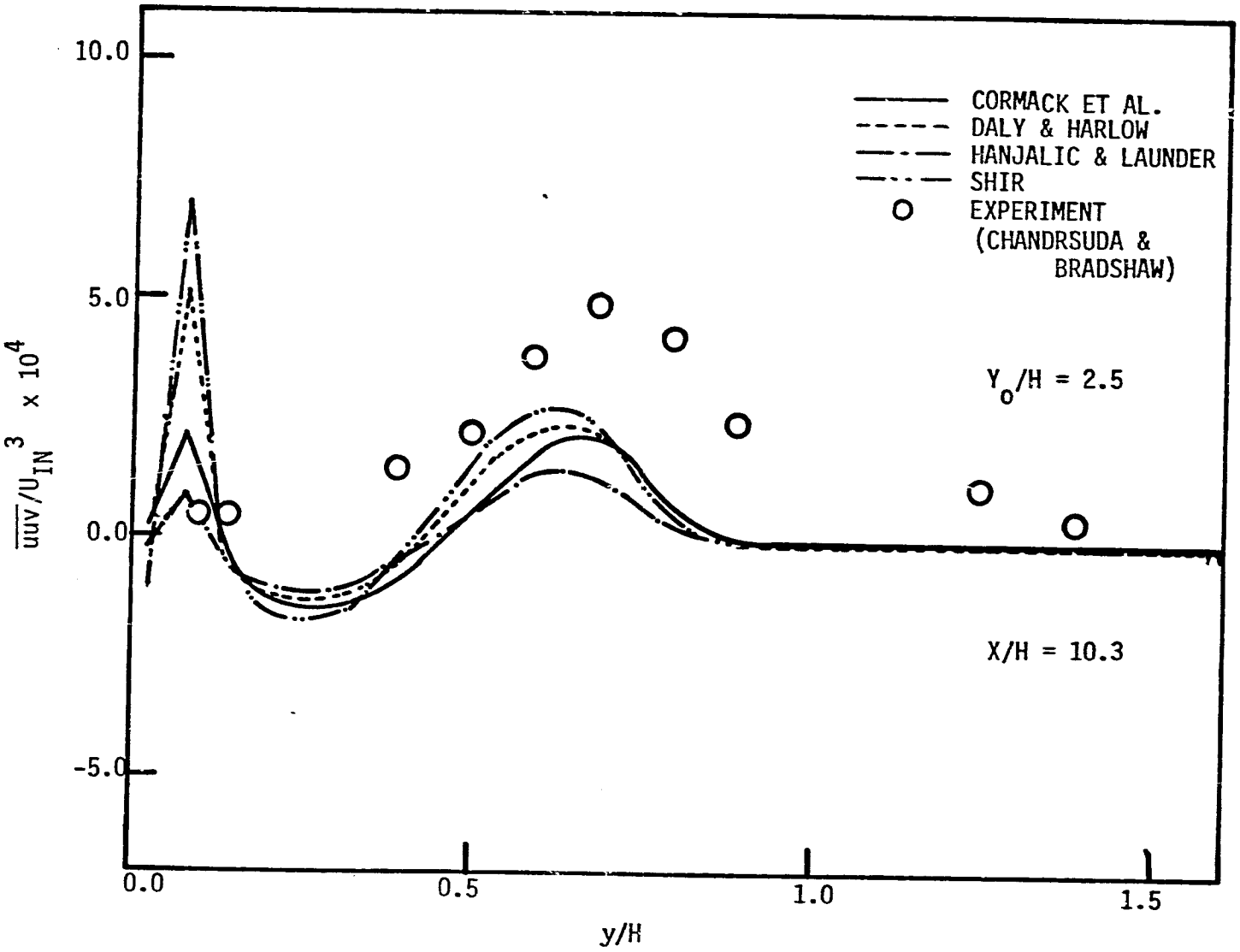

Figure 13 Triple velocity products at x/H = 10.3.
(comparison with experiment of Chandrsuda and Bradshaw)

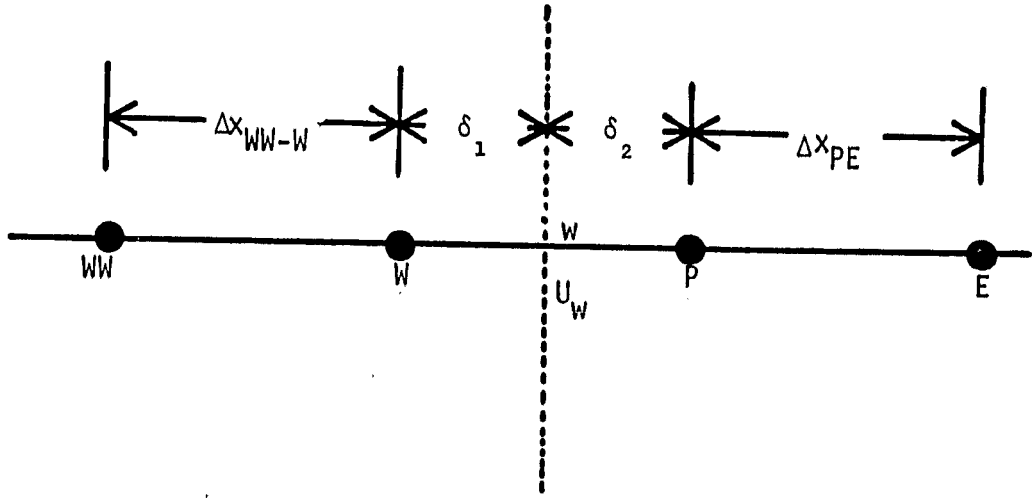

Figure 14 QUICK for non-uniform grid.